Building block analysis of 2D amorphous networks reveals medium range correlation

Christin Büchner [a], Liwei Liu [b,1], Stefanie Stuckenholz [a], Kristen M. Burson [a], Leonid Lichtenstein [a], Markus Heyde [a,*], Hong-Jun Gao [b], Hans-Joachim Freund [a]

[a] Fritz-Haber-Institut der Max-Planck-Gesellschaft, Faradayweg 4-6, 14195, Berlin, Germany
[b] Institute of Physics, Chinese Academy of Sciences, P.O. Box 603, Beijing 100190, China

ARTICLE INFO

ABSTRACT

The random network theory has been the long-accepted structural model for silica glasses. Now, a large bilayer silica sheet that was recently imaged with STM in atomic resolution provides the opportunity for real space structure analysis. General patterns in the formation of amorphous structures may be identified by looking at larger building blocks beyond single rings. Assessments of ring arrangements around each Si atom and ring neighborhoods are compared against uncorrelated structure predictions. A theoretical model of a two-dimensional silica network is investigated in parallel. Significant deviations of the observed structures from the uncorrelated prediction correspond qualitatively with a simple geometric approximation for bond angle frustration.

© 2016 Elsevier B.V. All rights reserved.

1. Introduction

Amorphous materials, also referred to as vitreous materials in the case of oxide glasses, are described structurally as random networks. This term refers to W. H. Zachariasen's postulate [1], that amorphous materials generally consist of the same building blocks as their crystalline counterpart, but with random connecting angles. This interpretation helped explain results gained by X-ray diffraction, the main source for atomic position data in that time. In pair correlation functions derived from diffraction, a sharp first peak is explained by uniform nearest neighbor (NN) distances in the basic building unit. This is true for both crystalline SiO_2 (quartz) and amorphous SiO_2 (glass), which indicates that the common primary building units are SiO_4-tetrahedra. At larger radii, the pair correlation function for amorphous materials exhibits increasingly broad and hard-to-identify peaks. Hence, diffraction experiments corroborate the hypothesis of equivalent small building units, but provide no direct clues on larger building blocks. Zachariasen concluded that the tetrahedral building blocks connect through shared corners to form a network of different sized pores [1]. These pores are of interest when silica is used as a support for catalysts and the active

species adsorb inside them. In the two-dimensional representation chosen by Zachariasen, the pores appear as rings of different sizes; for example, a five-membered ring is highlighted in the network schematic in Fig. 1(a).

Since diffraction techniques due to their averaging character could only provide limited insight on materials without long-range order, researchers have tried extensively to develop models for amorphous networks. A. C. Wright and M. F. Thorpe [2] give a brief overview on the historic development from tabletop models to computer simulations, as well as the discrepancy with experimental data that still remains today. One of these models consists of a triangle raft [3] directly based on the structural considerations presented by W. H. Zachariasen. An algorithm was employed to build a two-dimensional model structure from triangular building blocks. A large raft created in this way was presented in [3] and allows us to analyze the topology of an extended 2D unordered ring network. From this raft, J. F. Shackelford et al. derived a lognormal probability distribution of the ring sizes, which they postulated as being "an inherent feature of the connectivity requirements of the two-dimensional random network structure" [3].

Similar ring neighborhoods can also be observed in natural macroscopic networks and have garnered attention for roughly a hundred years [4]. For example, ephitelia (surface tissue) of plants and animals were compared as macroscopic examples of polygonal networks without long-range order [5]. A general tendency of many-sided rings to have few-sided neighbors, and vice versa was pointed out already by
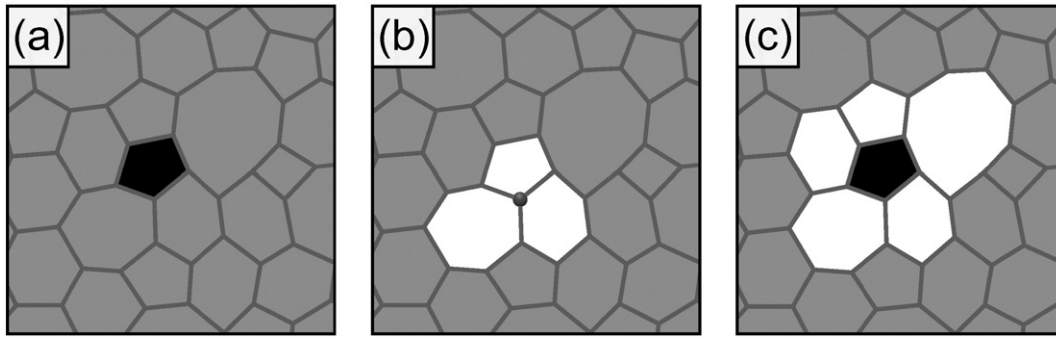

Fig. 1. Schematic representation of a two-dimensional amorphous silica network defining different building blocks: (a) single ring: each vertex or corner is the position of a silicon atom; (b) triplet: three rings sharing a silicon atom; (c) one central ring and all neighboring rings that share an edge.

F. Lewis [5]. It was D. A. Aboav, however, who first tried to describe this preferred arrangement quantitatively, albeit using empirically achieved factors, in what is now known as the Aboav–Weaire law [6].

Recently, real space data were presented on a continuous random network with the use of modern scanning tunneling microscopy (STM) [7] and corroborated independently with transmission electron microscopy (TEM) [8]. In both cases, an ultrathin SiO_2-film was prepared on an atomically flat surface. The film consists of just two atomic layers which are structurally identical and connected via perpendicular oxygen bridges. The layers are comprised of rings of different sizes, yielding random structures in the x,y-plane (image plane). This is a two-dimensional random network of SiO_2. Since W. H. Zachariasen chose a two-dimensional representation for his postulates, the resemblance to the experimental results is very striking. For relating the two-dimensional model system to three-dimensional materials, pair distance histograms (PDHs) are useful. For bulk materials, PDHs can be derived from diffraction experiments, whereas atomically resolved images allow direct measurement of interatomic distances. A histogram of all atom pair distances for the SiO_2 bilayer system shows two sharp peaks for the tetrahedral building unit, followed by increasingly broad peaks for next neighbor distances. Complete disorder (meaning constant probability to find another atom) only sets in at larger radial distances [7]. These features resemble the PDH plots for bulk materials from neutron diffraction (ND) and X-ray diffraction (XRD) [9,10].

Using the two-dimensional film as a model for amorphous structures allows us to study larger building units, i.e. rings and clusters of several rings in real space. We compare the structure of a large image of an amorphous SiO_2 network (403 rings) with a triangle raft (300 rings) in order to establish basic patterns for amorphous networks. We present quantitative analysis of single ring sizes (marked in Fig. 1(a)), as well as progressively larger building units, namely the ring arrangements around each Si atom (Fig. 1(b)) and ring neighborhoods (Fig. 1(c)). Histograms of ring sizes in each of these frameworks will be presented. We discuss the non-Gaussian distribution of single ring sizes and Euler's characteristic which can be used to assign a deforming contribution to each ring size.

Based on single ring size histograms, occurrence probabilities for each ring size are determined and used for predicting triplet and neighborhood combinations. The predicted uncorrelated combinations are compared against observed combinations and the influence of geometrical frustration is discussed. We categorize triplet combinations using a simplified geometric factor that is called the 'angle error'. For the ring neighborhoods, the Aboav–Weaire law is applied to predict neighborhoods and compared against observed neighborhoods.

2. Methods and theoretical background

A bilayer SiO_2 film was prepared on a Ru(0001) support, according to the recipe in [11]. STM images were taken using our custom built STM/AFM-setup [12]. Fig. 2(a) shows atomic resolution of the Si

positions. A closed chain of n vertices formed by Si atoms is called an n-membered ring (nMR) or a polygon with n vertices (i.e., pentagon, hexagon etc.). Rings of different sizes are indicated in Fig. 2(b) with different colors. The entire image consists of 403 rings, with ring sizes ranging from four to nine membered rings. Complete neighborhood data can be retrieved for 317 rings (also see supplement, Fig. S1). Statistics of ring sizes, ring size combinations and neighborhoods were counted manually, based on the atomic positions.

The creation of the triangle raft was described in [3,13]. The size of the loops thus created was limited from four to eight building blocks. The geometrical distortion of each ring was also limited. A large triangle raft of 300 rings was published in [13]. A cutout of this triangle raft is presented in Fig. 2(c) (full network data in supplement). The triangle corners correspond to oxygen positions; the center of each triangle corresponds to a silicon position. Rings of different sizes are indicated in Fig. 2(d) with different colors. Complete neighborhood data can be retrieved for 237 rings (also see supplement, Fig. S2). Statistical evaluations are provided in comparison with the silica network.

The neighborhood of a 2D network of polygons has been investigated many times before, be it at natural rock formations like the Giant's Causeway or the early studies of cell networks with optical microscopy [5]. D. A. Aboav [6] was the first to suggest an empirical formula for predicting the average size of neighboring grains m_n, based on the central grain's size n. This dependence was developed in the following years with different constants empirically found on various systems (a detailed account of this evolution can be found in [14]), and the resulting Aboav–Weaire law is usually expressed as

$$m_n = (6-a) + \frac{(6a + \mu_2)}{n} \tag{1}$$

with the empirical constant a taking different values depending on the system. Mostly values from 0 to 2 have been suggested, with most recommendations being close to 1 [15]. Comparative studies on soap foams [16], metallic glasses [17] and chalcogenide glasses [18] even lead to the declaration of $a = 1.2$ as a universal fit factor, expressing "a general property of naturally occurring nets" [17] as opposed to artificially constructed tessellations. Via the system's variance μ_2, the ring size distribution is included in the model (for more information on ring size distributions' variance μ_2, see [19]). Multiplication by n gives

$$m_n \cdot n = n(6-a) + (6a + \mu_2) \tag{2}$$

This linear dependence can be plotted and evaluated conveniently for different systems. We will use this empirical law to predict ring neighborhoods and compare this prediction to observed ring neighborhoods.
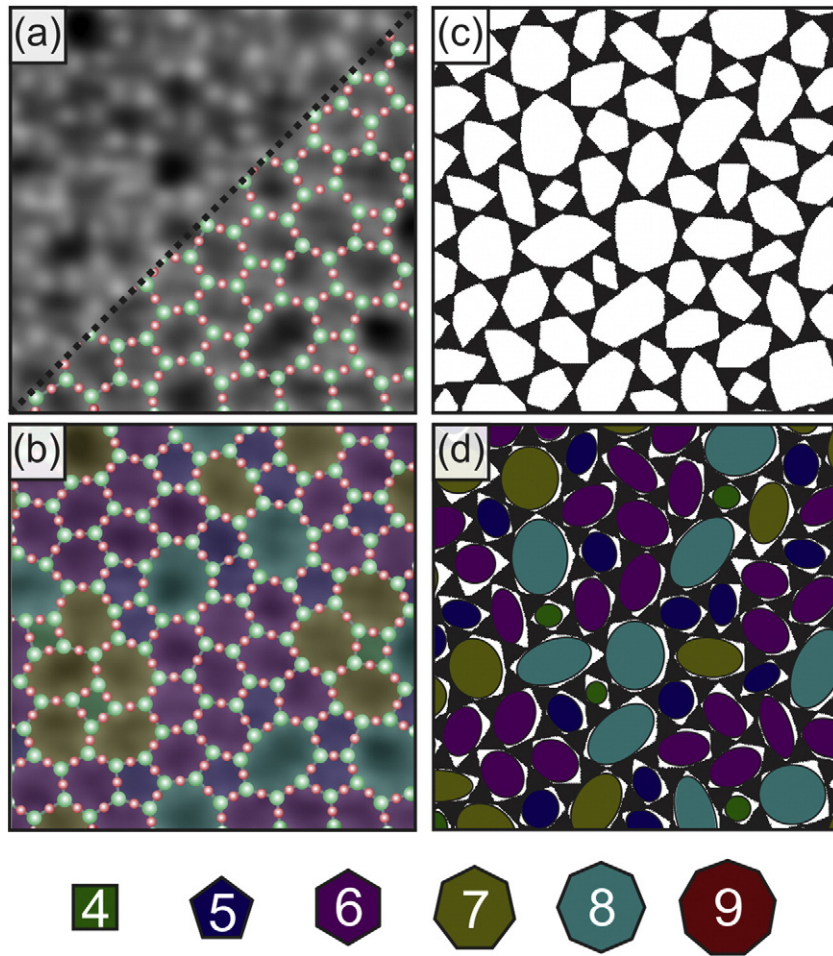
Fig. 2. (a) STM of two-dimensional SiO_2 ring network, size: 4 nm × 4 nm, recorded at $V_S = 2$ V, $I_T = 50$ pA. Rings of different sizes are arranged to fill the plane. On half of the image, atomic positions are indicated with green (Si) and red (O) spheres, respectively. (b) Dataset from (a), all atomic positions and ring sizes are visualized in individual colors. (c) Cutout of triangle raft network, published by J. F. Shackelford [13]. An algorithm creates arrays of triangles, corresponding to Zachariasen schematics. (d) Dataset from (c), ring sizes are indicated with colored ellipsoids.

3. Results

The tetrahedral SiO_4 building unit has been discussed in detail before [7]. It is identical for crystalline and amorphous SiO_2. Only the combination of two or more tetrahedra leads to structures that allow discrimination between amorphous and crystalline. The different structures are explained by a fixed bridging angle in the crystal and the flexible angle in the amorphous material [20]. Another prominent feature of the amorphous network is the presence of differently sized rings that fill the plane. Due to their irregular shapes, they amount to broad, hard-to-interpret features in diffraction based, averaging experiments like XRD. Real space information, however, now enables us to investigate the network of rings, just like a light microscope enables the study of cell networks in plant tissue. For the silica film and the triangle
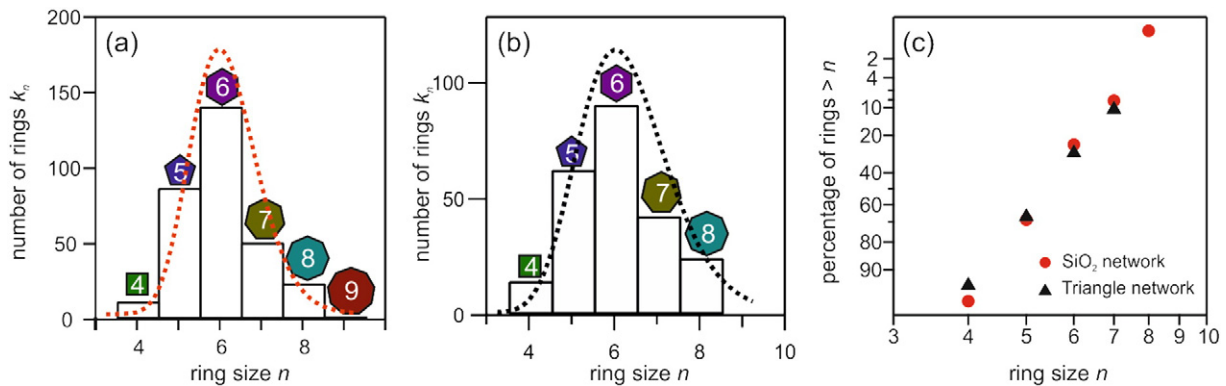

Fig. 3. (a) Ring size distribution of an amorphous SiO_2 network (317 rings, partly shown in Fig. 2(a)). (b) Ring size distribution of Shackelford's triangle raft (237 rings, partly shown in Fig. 2(c)). The bars in each histogram are labeled with the according ring size. Red/black dashed curves indicate a lognormal fitting function. (c) Lognormal probability plot of the ring sizes. Red circles correspond to SiO_2, black triangles correspond to the triangle network. Both distributions exhibit a linear behavior when plotted in this way.

raft investigated in this study, ring size histograms are shown in Fig. 3(a) and (b), respectively. In the two-dimensional silica film, the ring sizes range mostly from four to nine, whereas the sizes in the triangle raft were limited by the algorithm from four to eight. In both systems, the five-membered rings are more abundant than the seven-membered rings, while the eight membered-rings occur more frequently than the four-membered rings. This order is in qualitative agreement with the relative energies of the isolated silica double rings calculated by DFT [7].

It is a general tendency observed throughout many different silica images, that the ring size distribution does not follow a Gaussian distribution, but appears to be asymmetric with respect to the most abundant species, which is the six-membered ring. This distribution can be described by using a log-normal distribution function, which exhibits a linear behavior in a log-normal probability plot (Fig. 3(c)). It was shown before, that two-dimensional networks, which (i) are amorphous and (ii) have a narrow range of bond distances between the tetrahedral blocks, generally show a lognormal distributions of their ring sizes as an inherent structural property [19].

The combination of three rings that share one Si atom will now be investigated (compare Fig. 1(b)). Using the *individual* probabilities for each ring size derived from Fig. 3, a *combined* occurrence probability

for each triplet combination can be predicted. The probability of each triplet combination simply equals the product of the single ring probabilities, with a factor multiplier accounting for different possible permutations of klm combinations where $k \neq l \neq m$, $k = l \neq m$ or $k = l = m$, respectively (details in the supplement). The uncorrelated expectation for each possible triplet is set against the real count (in black bars), corresponding to the triplet combinations that are observed in the STM image of the SiO_2 bilayer (Fig. 4(a)) and the Shackelford raft (Fig. 4(b)). All observed combinations are plotted from left to right in ascending order of the prevalence of real counts. Only complete triplets were counted for this statistic, omitting silicon atoms at the edge of the image.

The "expected counts" are normalized for the size of the ring network and plotted in Fig. 4(a) for the SiO_2 network, and Fig. 4(b) for the triangle raft. However, they represent merely a statistical consideration, assuming that all rings present in the network can randomly (meaning without correlation) arrange to tile the plane. Yet, the fact that neither gaps nor overlaps are observed in the plane, indicates that a geometric condition also needs to be met for the arrangement of rings. The rings sharing an atom must fill out the plane entirely, the sum of their inner angles covering 360°. When we calculate the difference between 360° and
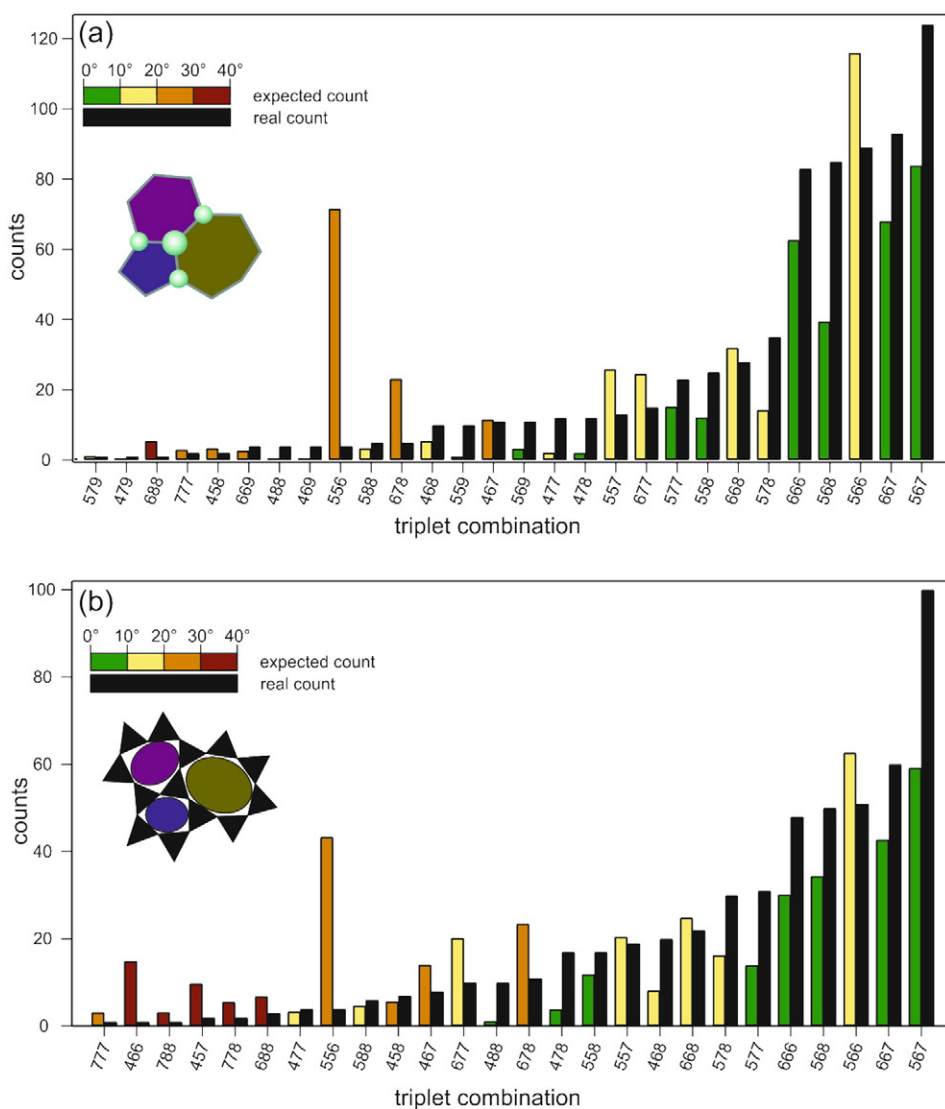

Fig. 4. Ring triplet occurrence. Statistically predicted occurrence of ring triplet combinations (colored bars) versus observed combinations (black bars) for SiO_2 network (a) and Shackelford network (b). All combinations that actually occur are shown in ascending order of occurrence. The color of the predicted occurrence corresponds to the magnitude of absolute angle error in each combination.

the sum of inner angles assuming ideal polyhedra, we can assign an "angle error"

$$\Delta_{klm} = |360° - (\alpha + \beta + \gamma)| \qquad (3)$$

to each triplet combination of ring sizes k, l and m with ideal internal angles of α, β and γ. Δ_{klm} theoretically can take values from 0° (for the combination of three six-membered rings) to 90° (for the combination of three four-membered rings). The bars for the expected count are marked in different colors representing the absolute value $|\Delta_{klm}|$ in four increments for no or little angle error (green bars), medium angle error (yellow), and higher angle error (orange and red bars). The largest absolute angle error observed is 30° (33° in case of the triangle raft), with the most strained ring combination being a 688-triplet. Combinations with larger Δ_{klm} are not observed, even if they possess high statistical probability. The implication of this angle error will be addressed further in the Discussion section.

In order to examine the Aboav–Weaire law discussed in the literature, we determined the rings occurring in the neighborhood of four-membered rings, five-membered rings etc. We define ring neighbors as two rings sharing two Si atoms, or an edge. The results are shown in Fig. 5 for the silica network and in Fig. 6 for the Shackelford network. For each central ring size, a separate histogram (black bars) shows the ring sizes that share an edge with the central ring. The rings at the border of each network were not counted as central rings, but only as neighbors to inner rings [also see Fig. S1 in supplement]. This can be first compared to the predicted random neighborhood, which has been created from the individual ring statistics, assuming an uncorrelated system. From this assumption follows, that on average all rings will have the same neighborhood. This distribution of neighbors is derived from the single ring distribution by scaling for the amount of edges at each ring (each ring of size n possesses n edges). All k_n rings of size n together have $k_n \cdot n$ ring neighbors and their size distribution is proportional to the previously determined neighbor distribution. This random neighbor distribution is indicated in Figs. 5 and 6 in gray bars.

Next to each histogram pair, the angle error $\overline{\Delta}_{corner}$ is indicated. It is calculated according to Eq. (3) for each Si atom of the central ring, then averaged for all atoms. We give the distributions of these values in the supplement, and provide the mean value here in the respective graph. In this case, the sign of each angle value was preserved, however, to express how the bond angles in this arrangement typically have to bend to accommodate smaller or larger angles, respectively. The results are in agreement with the intuitive understanding of polygons filling the two-dimensional space. In case of small central rings (four-membered or five-membered), the bond angles at each silicon atom have to stretch wider with respect to each polygon's ideal internal angle in order to fill the plane. In case of central rings larger than six-membered, a positive angle error is calculated, which corresponds to the polygon internal angles being compressed (with respect to the symmetric polyhedron) to fit into the plane.

4. Discussion

We have quantitatively analyzed the building blocks of two amorphous network structures at increasing length scales: first single rings, then triplets of rings and, finally, the complete neighborhood around each ring. Different laws have been suggested about the formation of these structures. Our real space data enable us to investigate the formation principles for amorphous networks.
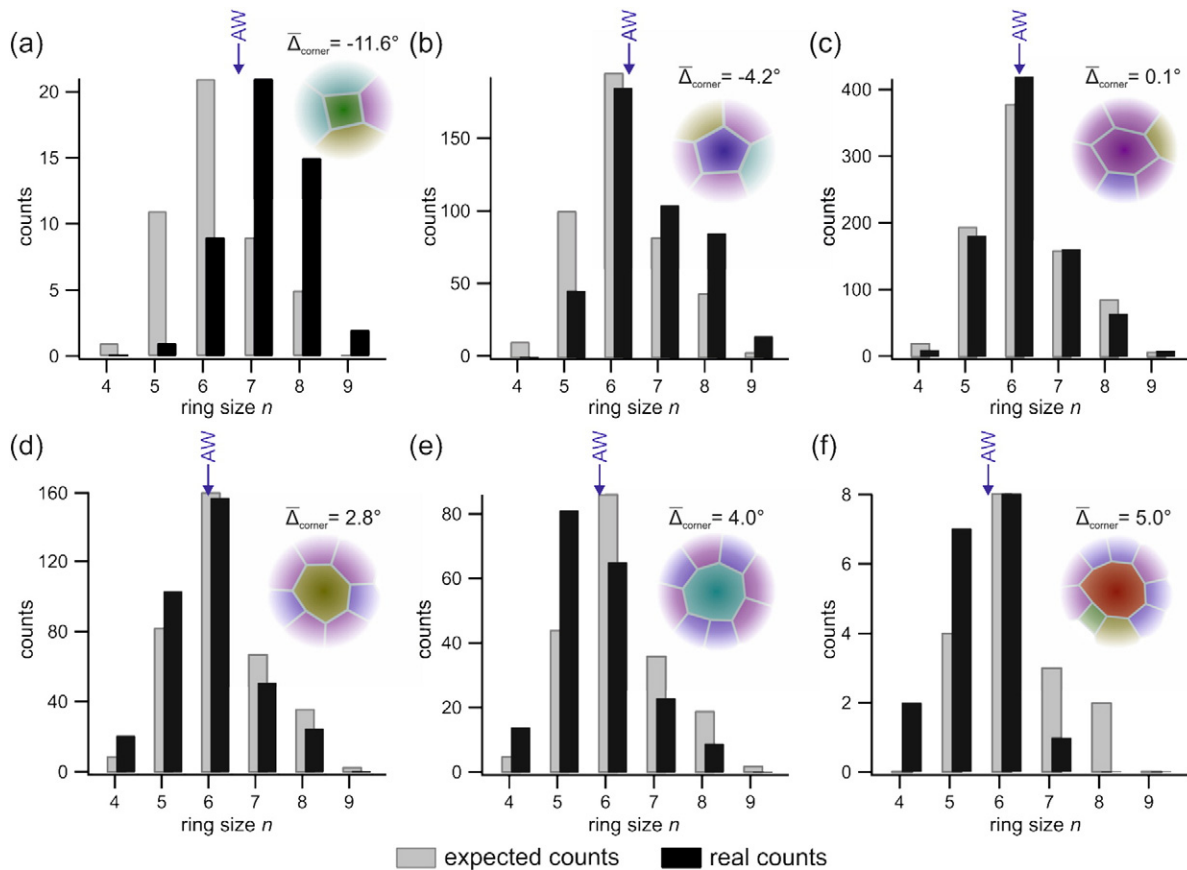

Fig. 5. Ring neighborhood evaluation for SiO₂. (a) histograms of rings surrounding 4MR, gray bars for prediction, black bars for real count. $\overline{\Delta}_{corner}$ denotes the mean value for the angle error, averaged for all 4MR. A blue arrow ("AW") indicates the predicted mean for the neighborhood of 4MR according to the Aboav–Weaire law. The same quantities are given for 5MR (b), 6MR (c), 7MR (d), 8MR (e) and 9MR (f).
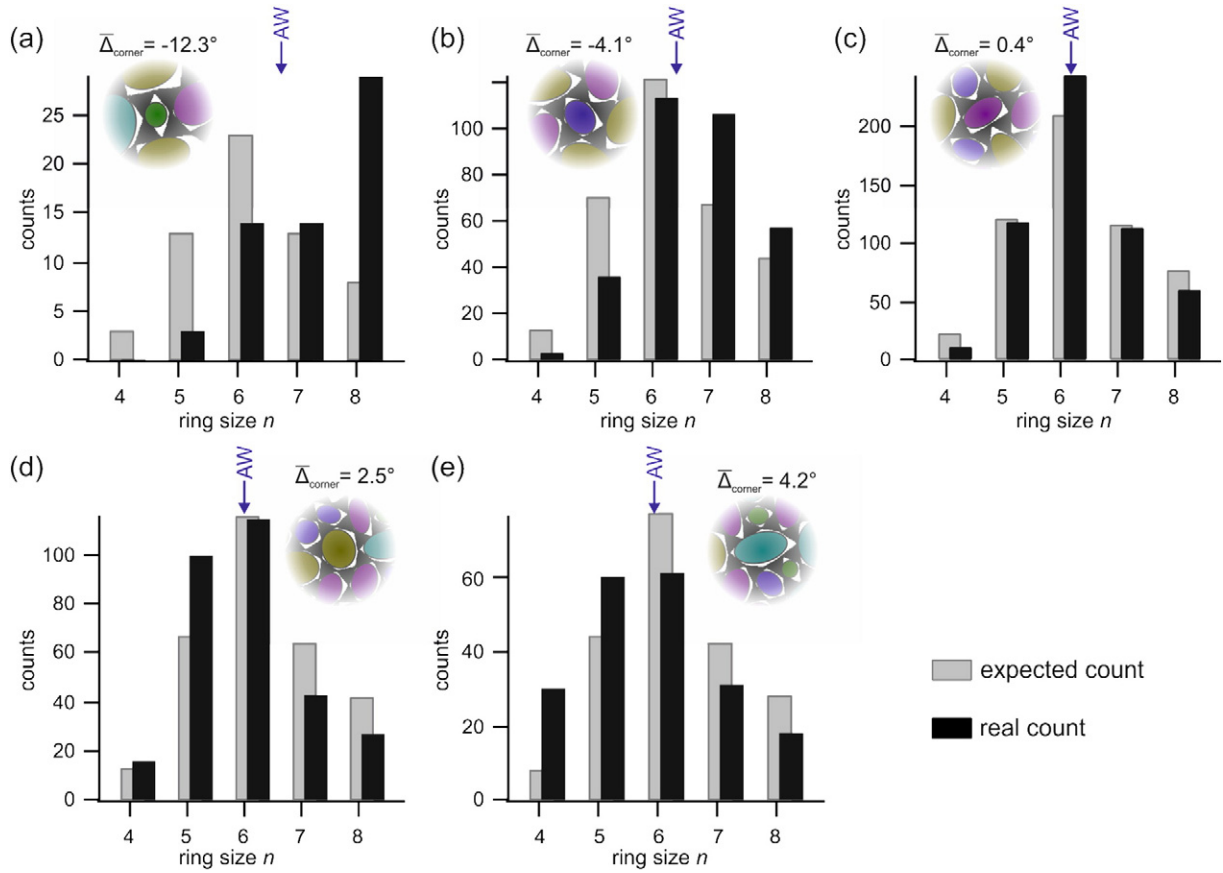
Fig. 6. Ring neighborhood evaluation for Shackelford's network. (a) histograms of rings surrounding 4MR, gray bars for prediction, black bars for real count. $\overline{\Delta}_{corner}$ denotes the mean value for the angle error, averaged for all 4MR. A blue arrow ("AW") indicates the predicted mean for the neighborhood of 4MR according to the Aboav-Weaire law. The same quantities are given for 5MR (b), 6MR (c), 7MR (d) and 8MR (e).

Starting conceptually from an ordered two-dimensional network of hexagons, we can determine the structural influence of rings that deviate from $n = 6$. In accordance with the Euler characteristic connecting an object's faces, edges and vertices, a network filling a two-dimensional flat plane needs to have zero overall curvature. Despite the asymmetric ring size distributions shown in the ring size histograms (Fig. 3(a) and (b)), the combined structural influences from small and large rings compensate one another. A five-membered ring introduces a certain curvature, which is exactly counterbalanced by the curvature resulting from a seven-membered ring. The structural modification from a four-membered ring is balanced by an eight-membered ring (or two seven-membered rings) and so on. Discussing ring size influence on a graphene sheet, T. W. Ebbesen [21] derived from Euler's expression a simple sum rule

$$\sum (6-n)k_n = 0 \qquad (4)$$

which expresses the overall curvature in the system and can be employed for our 2D networks as well. Here, k_n is the number of all rings of size n. An ideal flat structure will achieve $\Sigma = 0$, since any curvature induced by one building block is balanced by another block with opposite curvature. The silica film presented here yields a sum of $\Sigma_{Silica} = -6$, the Shackelford network yields $\Sigma_{Shackelford} = 0$. The deviation from 0 in the case of the silica network must be interpreted as a sampling size effect, as the deviation per ring steadily decreases with increasing number of rings considered.

Instead of condensing the structural influence of all rings into one number, we now look at individual clusters of rings to identify the characteristics of these network structures better. From comparing the occurrence of triplets (Fig. 4) and ring neighborhoods (Figs. 5 + 6) with the prediction based purely on random arrangements of individual rings, it is quite clear that the 2D amorphous network structure is not an uncorrelated system. Closer scrutiny of ring triplets can give an indication of the driving forces for this system.

We have predicted a statistical probability for each triplet combination (expected counts: color coded bars) and compared them to the data (real counts: black bars) from our image in Fig. 4. This very simple model correctly predicts the combinations 567, 667, 566, 568 and 666 to occur significantly more than all other combinations. We focus more strongly on these combinations for measuring the success of the uncorrelated prediction, since they together make up 66% of all combinations (58% for the triangle raft). Therefore, a good statistical base is provided for those combinations. However, the random model also predicts the combination 556 to occur much more frequently than it actually does, in fact it is predicted to be the third-most-likely combination. For both the silica and the Shackelford system we observe this trend. Also, within the group of the five most probable combinations, the random model will not predict their order correctly.

These limitations indicate that the amorphous networks are in some way correlated, rather than completely random in their arrangement. We can begin to understand this discrepancy by introducing a geometrical consideration into our model. This is done by estimating the angle error, Δ_{klm} (Eq. (3)), as introduced in the previous section. Analyzing the real versus the expected counts together with the angle error, the combinations can be discussed within certain categories. In Fig. 4, the expected count bars are color coded green for very small (from 0° to under 10°), yellow for medium (from 10° to under 20°) and in orange (from 20° to under 30°) and red for larger angle errors (30° to 40°). Here, we only focus on the absolute value of Δ_{klm}, signs and individual values are provided in the supplement.

This additional parameter gives an indication why certain combinations, such as 567, occur more often than predicted. They are favored due to their small geometric strain. In fact, all combinations with angle errors below 12° exhibit larger real counts than the random expectation. This holds for both networks, the silica film as well as for the Shackelford model. From the aforementioned first five combinations that make up the majority of triplets, only the combination 566 possesses an angle error larger than 10°, and occurs in a smaller amount than predicted. For the category of medium angle error (yellow bars), the random expected counts do not exhibit a general trend. Instead, some combinations are over- and others underestimated with respect to real counts. On the other hand, all the combinations that have an estimated angle error of 22° or more (>27° for the triangle raft), that is, highly frustrated bond angles, occur less often than predicted. These are color coded in orange and red. This can be nicely seen in both network structures especially for the 556 and 678 combinations.

We find that the angle error is a simple tool that serves to define regions of strong geometric favorability (low error value) and strong disfavorability (high error value) where the probability of forming the respective triplet combinations strongly deviates from an uncorrelated, random behavior. A similar trend can be discovered when the Euler sum according to Eq. (4) is considered for each triplet combination (all values in supplement, Table S3). A small value indicates that the triplet is largely flat and any curvature induced by larger rings is balanced by smaller neighbors. For all triplet combinations which occur more than 10 times, this local Euler sum has an absolute value of 2 or smaller, while the maximal value for an observed combination is 4, and the hypothetical maximum is 9. This indicates that the combinations with small absolute local Euler sum are less strained in terms of the flat 2D character of the system. Further analysis is needed to uncover additional parameters and develop a predictive model for the formation of triplet building units.

Moving from ring triplets to the next larger building unit, namely the ring neighborhood (compare Fig. 1(c)), we can use similar tools to analyze the formation principles of our network. Fig. 5 shows the neighborhoods for each ring size in the silica film, Fig. 6 for the triangle raft. The prediction (gray bars) represents the entire ring edge distribution, scaled for the share of edges that each ring size possesses. Analogous to the model previously used for the triplet combinations, this prediction assumes that rings arrange randomly on the plane without other factors than occurrence probability influencing these arrangements. In comparing the prediction to the observed neighborhoods (black bars), we find that other factors do seem to influence the arrangements. The general tendency of few-sided polygons to preferably have many-sided neighbors is observed in both the silica and the triangle raft. The mean value for surrounding rings of each observed ring neighborhood decreases as the central ring size increases. The opposite is true for the mean angle error. The angle error is determined according to Eq. (3) for each Si atom involved in the central ring. A mean value $\overline{\Delta}_{corner}$ is indicated in each histogram, representing the averaged Δ_{klm} for all Si atoms involved in the respective central ring size. A small central ring typically exhibits negative angle errors, meaning the bond angles need to expand from their *ideal* internal angles to fill the plane. When the central ring is larger, the bond angles, on average, are contracted instead, which is expressed by a positive angle error $\overline{\Delta}_{corner}$.

The polygon neighborhood has been previously investigated for macroscopic networks and is generally described with the empirically found Aboav–Weaire law. This relation was originally developed to describe macroscopic systems like cell networks in plant tissue; it is therefore intriguing to apply it to an atomically amorphous system in which building blocks are determined by rigid interatomic bond lengths and angles. The Aboav–Weaire law predicts an average neighbor size m_n for each ring size n. Besides the network's variance μ_2, this model only uses a fitting factor a. The predicted mean neighbor sizes are indicated

for the silica network in Fig. 5 and for the triangle raft in Fig. 6, respectively. The real space ring neighborhood information gathered from our imaging technique allows reviewing the validity of this general law for the case of atomically defined amorphous networks, since we can determine the actual average neighbor size.

In order to highlight how well the Aboav–Weaire law holds for the two investigated networks, we use its linear expression which was derived in Eq. (2). Fig. 7 shows the observed ring neighborhoods of the silica network and the Shackelford triangle network; $(m_n \cdot n)$ is plotted against n. Red data points represent the experimentally determined average neighbor size m_n for each central ring size n in the silica film. An error bar on each data point gives the standard deviation of the distribution of neighbor rings. A red curve represents the linear fit to the data. For the triangle raft, the analogous data are plotted in black. The blue curve shows the Aboav–Weaire prediction according to Eq. (2), with the value 1.2 chosen for a (declared to hold in general for naturally occurring networks [17]) and $\mu_2 = 0.95$ (variance value of the silica network). In the case of the triangle raft, an analogous Aboav–Weaire prediction only differs through the variance μ_2 and results in a parallel line with a slight offset. It is therefore not shown in Fig. 7 to improve legibility. It is striking that the prediction of a linear dependence holds for both systems investigated. Both the silica and the triangle network can be fitted with a linear function according to Eq. (2), from which the fitting parameters a and μ_2 can subsequently be derived (see Table 1). In both cases the μ_2 value calculated from the ring statistics and the μ_2 value derived from the neighborhood fit are in good agreement. However, the fitting values for a deviate significantly from 1.2, which might be a characteristic for networks governed by rigid interatomic bond lengths. With real space data from more covalent networks, a general framework for the Aboav–Weaire law including a better physical assignment for the parameter a may be obtained in the future.

5. Conclusion

We have investigated the network structure of two models of amorphous silica, an experimental bilayer of SiO_2 on a Ru(0001) support and a simulated triangle network. Real space data provide an insight into
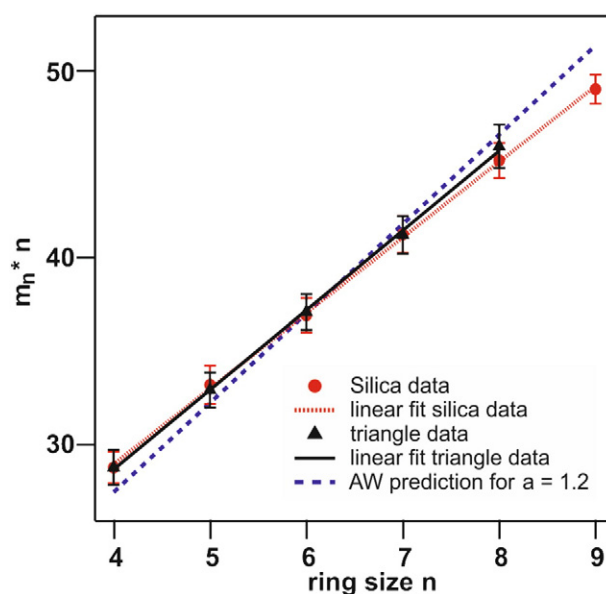

Fig. 7. Aboav–Weaire's law of polygon neighborhoods. Red circles correspond to the average neighbors observed in the network of silica rings. Black triangles correspond to the average neighbors observed in Shackelford's triangle network. A linear fit is well suited to describe both datasets (red line and black dotted line). The fitting parameters are given in Table 1. The blue line shows the theoretical prediction according to Eq. (2) with $a = 1.2$ (suggested universal fit parameter) and $\mu_2 = 0.95$ (variance of silica network).

Table 1

Fitting parameters μ_2 and a for silica bilayer and triangle raft, in comparison with real variance μ_2.

System	μ_2 (real space data)	μ_2 from fit (Fig. 7)	a from fit (Fig. 7)
Silica bilayer	0.95	0.97 ± 0.01	1.94 ± 0.05
Triangle raft	1.08	1.13 ± 0.01	1.72 ± 0.07

building units beyond the tetrahedral SiO_4-block. Using this data, we review the established description of silica glasses as continuous random networks. To this end, we have studied single rings, ring triplets and ring neighborhoods. The distributions of ring sizes follow a log-normal distribution for both systems. Ring sizes smaller than six introduce a distortion into the system which is balanced by larger rings. This property can be captured in Euler's characteristic. Larger building units have been investigated to learn more about the factors influencing ring arrangements in amorphous structures. Ring triplets sharing one Si atom have been studied in comparison with a random model, assuming no correlation. Adding the angle error as a geometric factor to this model helps to understand why some combinations are geometrically favorable and therefore underestimated by the random model and vice versa. However, more theoretical investigations are needed in order to develop a predictive model for the formation of extended network structures.

While the angle error relies on a simplified geometric model, it is a quick means to show that formation of ring neighborhoods is likewise not an uncorrelated process, but influenced by geometry. Strain or induced curvature can be balanced by a neighboring building block of opposite structural influence. Further investigations are needed to elucidate how geometrical strain is alleviated through progressively larger building units. Typical building blocks of medium range may be identified, through which the energy of the system is minimized. The observed average size of neighboring rings was compared against the prediction from Aboav-Weaire's law, revealing that the universally assumed linear relationship of $m_n \cdot n$ vs n seems to hold not only for macroscopic cell networks, but also for an amorphous network made up of covalent bonds.

Acknowledgment

Appendix A. Supplementary data

Supplementary data to this article can be found online at http://dx.doi.org/10.1016/j.jnoncrysol.2015.12.020.

References

[1] W.H. Zachariasen, The atomic arrangement in glass, J. Am. Chem. Soc. 54 (1932) 3841–3851, http://dx.doi.org/10.1021/ja01349a006.

[2] A.C. Wright, M.F. Thorpe, Eighty years of random networks, Phys. Status Solidi Basic Res. 250 (2013) 931–936, http://dx.doi.org/10.1002/pssb.201248500.

[3] J.F. Shackelford, B.D. Brown, The lognormal distribution in the random network structure, J. Non-Cryst. Solids 44 (1981) 379–382, http://dx.doi.org/10.1016/0022-3093(81)90040-5.

[4] D.W. Thompson, On Growth and Form, Cambridge [Eng.] University Press, Cambridge, 1917 (https://archive.org/details/ongrowthform1917thom).

[5] F.T. Lewis, A comparison between the mosaic of polygons in a film of artificial emulsion and the pattern of simple ephithelium in surface view (cucumber epidermis and human amnion), Anat. Rec. 50 (1931) 235–265, http://dx.doi.org/10.1002/ar.1090500303.

[6] D.A. Aboav, The arrangement of grains in a polycrystal, Metallography 3 (1970) 383–390, http://dx.doi.org/10.1016/0026-0800(70)90038-8.

[7] L. Lichtenstein, C. Büchner, B. Yang, S. Shaikhutdinov, M. Heyde, M. Sierka, et al., The atomic structure of a metal-supported vitreous thin silica film, Angew. Chem. Int. Ed. 51 (2012) 404–407, http://dx.doi.org/10.1002/anie.201107097.

[8] P.Y. Huang, S. Kurasch, A. Srivastava, V. Skakalova, J. Kotakoski, A.V. Krasheninnikov, et al., Direct imaging of a two-dimensional silica glass on graphene, Nano Lett. 12 (2012) 1081–1086, http://dx.doi.org/10.1021/nl204423x.

[9] R.L. Mozzi, B.E. Warren, The structure of vitreous silica, J. Appl. Crystallogr. 2 (1969) 164–172, http://dx.doi.org/10.1107/S0021889869006868.

[10] D.I. Grimley, A.C. Wright, R.N. Sinclair, Neutron scattering from vitreous silica IV. Time-of-flight diffraction, J. Non-Cryst. Solids 119 (1990) 49–64, http://dx.doi.org/10.1016/0022-3093(90)90240-M.

[11] L. Lichtenstein, M. Heyde, H.-J. Freund, The atomic arrangement in two dimensional silica — from crystalline to vitreous structures, J. Phys. Chem. C (2012)http://dx.doi.org/10.1021/jp3062866.

[12] M. Heyde, G.H. Simon, H.-P. Rust, H.-J. Freund, Probing adsorption sites on thin oxide films by dynamic force microscopy, Appl. Phys. Lett. 89 (2006) 263107, http://dx.doi.org/10.1063/1.2424432.

[13] J.F. Shackelford, Triangle rafts — extended zachariasen schematics for structure modeling, J. Non-Cryst. Solids 49 (1982) 19–28, http://dx.doi.org/10.1016/0022-3093(82)90106-5.

[14] S.N. Chiu, Aboav-weaire's and lewis' laws - a review, Mater. Charact. 34 (1995) 149–165, http://dx.doi.org/10.1016/1044-5803(94)00081-U.

[15] I. Zsoldos, A. Szasz, Appearance of collectivity in two-dimensional cellular structures, Comput. Mater. Sci. 15 (1999) 441–448, http://dx.doi.org/10.1016/S0927-0256(99)00031-2.

[16] D.A. Aboav, The arrangement of cells in a Net, Metallography 13 (1980) 43–58, http://dx.doi.org/10.1016/0026-0800(80)90021-X.

[17] D.A. Aboav, The arrangement of cells in a Net. II, Metallography 16 (1983) 265–273, http://dx.doi.org/10.1016/0026-0800(83)90012-5.

[18] D.A. Aboav, The arrangement of cells in a Net. III, Metallography 17 (1984) 383–396, http://dx.doi.org/10.1016/0026-0800(84)90075-2.

[19] C. Büchner, P. Schlexer, L. Lichtenstein, S. Stuckenholz, M. Heyde, H.-J. Freund, Topological investigation of two-dimensional amorphous materials, Z. Phys. Chem. 228 (2014) 587–607, http://dx.doi.org/10.1515/zpch-2014-0438.

[20] L. Lichtenstein, M. Heyde, H.-J. Freund, Crystalline-vitreous interface in two dimensional silica, Phys. Rev. Lett. 109 (2012) 106101, http://dx.doi.org/10.1103/PhysRevLett.109.106101.

[21] T.W. Ebbesen, Cones and tubes: geometry in the chemistry of carbon, Acc. Chem. Res. 31 (1998) 558–566, http://dx.doi.org/10.1021/ar960168i.